Quantum Many-Body Dynamics of Driven-Dissipative Rydberg Polaritons

Tim Pistorius,* Javad Kazemi, and Hendrik Weimer
Institut für Theoretische Physik, Leibniz Universität Hannover, Appelstraße 2, 30167 Hannover, Germany

(Received 25 March 2020; accepted 30 November 2020; published 30 December 2020)

We study the propagation of strongly interacting Rydberg polaritons through an atomic medium in a one-dimensional optical lattice. We derive an effective single-band Hubbard model to describe the dynamics of the dark-state polaritons under realistic assumptions. Within this model, we analyze the driven-dissipative transport of polaritons through the system by considering a coherent drive on one side and by including the spontaneous emission of the metastable Rydberg state. Using a variational approach to solve the many-body problem, we find strong antibunching of the outgoing photons despite the losses from the Rydberg state decay.

DOI: 10.1103/PhysRevLett.125.263604

The interplay between external driving and dissipation in strongly interacting quantum many-body systems leads to the emergence of rich nonequilibrium dynamics not found in closed quantum systems [1,2], yet their theoretical analysis is extremely difficult [3]. This is especially true in Rydberg polariton systems [4–16], where the metastable character of the Rydberg excitation provides a natural dissipative element. Here, we show that a variational analysis can successfully describe this challenging many-body problem.

Strongly interacting Rydberg polaritons are closely linked to the appearance of electromagnetically induced transparency (EIT) involving a highly excited Rydberg state [17,18]. Early experiments have observed a decline of the EIT feature due to strong Rydberg interactions [19,20]. More recent experiments have demonstrated the appearance of a strongly interacting polariton quasiparticle consisting of both light and atomic matter, in a many-body setting [6–8] as well as on the single polariton level [9–11], with immediate applications in the generation of strongly correlated photon states [21] and photonic quantum computing [12,22]. The theoretical analysis of these systems has so far been limited to an exact treatment of up to two interacting Rydberg polaritons [13], or to large quantum many-body simulations in the absence of the decay of the Rydberg state [14–16].

In this Letter, we investigate the driven-dissipative quantum many-body dynamics of Rydberg polaritons in an optical lattice potential. We derive the dispersion relations for the single particle problem, from which we obtain an effective Bose-Hubbard model for the dark-state polaritons with long-range hopping and long-range interactions arising from the van der Waals interaction of the Rydberg states. We show that under experimentally realistic conditions, the dynamics is confined to a single dark-state polariton band, even in the presence of dissipation from the decay of the Rydberg state and conversion of dark-state polaritons into bright polartions by the van der Waals interaction. We analyze the driven-dissipative many-body model using a variational approach, which we benchmark against wave-function Monte Carlo simulations for small system sizes. Finally, we show that strongly correlated photons can be observed when the polaritons are leaving the system.

We consider multiple ensembles of rubidium atoms in an effective one-dimensional (1D) geometry with length $L = Na$ with a being the spacing between the N lattice sites created by an appropriate optical lattice potential [23]. The atomic density $n(z)$ on each site is approximated by a Gaussian distribution with an average density of $n_0 = 10^{13}$ cm^{-3} and a standard deviation of $\sigma = 25$ nm. Figure 1 shows a depiction of $n(z)$ and the level structure of the trapped atoms. Two counterpropagating light fields E_+, E_- with the same polarization couple the ground state $|g\rangle$ to a single excited state $|e\rangle$ with a transition frequency of ω_{ge} and are described by the bosonic operators $\hat{\Psi}_{E_+}$ and $\hat{\Psi}_{E_-}$.

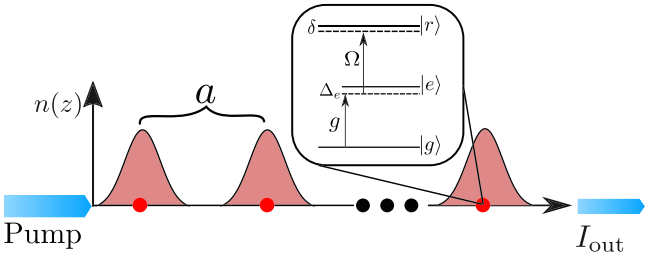

FIG. 1. Setup of the system for dark-state polariton propagation. A one-dimensional optical lattice potential creates lattice sites separated by a distance a, around which the atoms exhibit approximately Gaussian density profile. The system is being pumped from the left by a coherent light field, leading to an output intensity I_{out}. Each atom is driven by a photon field with a space-dependent coupling g and a coherent laser field Ω with a two-photon detuning δ. The photon field is detuned by Δ_e from the intermediate state.

The propagation in opposite directions allows for a description in terms of localized Wannier functions [24]. The light fields can be detuned by δ_e from the atomic transition which we combine with the linewidth γ_e of $|e\rangle$ to a complex detuning $\Delta = \delta_e - i\gamma_e$. A second (control) field with Rabi frequency Ω enables the transition to a Rydberg state $|r\rangle$ and is set to satisfy a two-photon resonance ($\delta = 0$) which brings our system into the EIT regime. The collective, single-photon Rabi frequency $g(z)$ in this regime is then given by

$$g(z) = \tilde{g}\sqrt{n(z)}\sum_l e^{i\tilde{k}la}, \tag{1}$$

with $\tilde{g} = [6\pi\gamma_e c^3/\omega_{ge}^2]^{1/2}$ and c being the speed of light [16]. We split the phase factor up in two parts by setting $\tilde{k} = k_0 + k'$ which corresponds to the wave vector $k_0 = \omega_{ge}/c$ and a deviation from the EIT condition k'. The transition processes within the atoms can then be described by the bosonic field operators $\hat{\Psi}_e = |g\rangle\langle e|$ and $\hat{\Psi}_r = |g\rangle\langle r|$ [15]. In the continuum, the noninteracting part of the Hamiltonian can then be written as

$$H_0 = \hbar\int dz \hat{\mathbf{\Psi}}^\dagger \begin{pmatrix} -ic\partial_z & 0 & g(z) & 0 \\ 0 & ic\partial_z & g(z) & 0 \\ g(z) & g(z) & \Delta & \Omega \\ 0 & 0 & \Omega & \delta \end{pmatrix} \hat{\mathbf{\Psi}}, \tag{2}$$

with $\hat{\mathbf{\Psi}} = \{\hat{\Psi}_{E_+}, \hat{\Psi}_{E_-}, \hat{\Psi}_e, \hat{\Psi}_r\}$. The kinetic terms for the quantized light fields only account for the previously mentioned deviation from the two-photon resonance.

We obtain the single polariton solution of Eq. (2) by using a Bloch wave ansatz $\boldsymbol{\phi}_k(z) = e^{ikz}\mathbf{u}_k(z)$ in combination with a plane wave expansion for the periodic functions $\mathbf{u}_k(z)$. The eigenstates of the resulting band structure are a composition of the previously defined bosonic fields and can be interpreted as polaritons [25]. Most eigenstates will dissipate quickly because of the spontaneous emission rate that arises from any contribution of $|e\rangle$. Hence, we want to focus on the dark-state polaritons with their vanishing population $\langle\hat{\Psi}_e^\dagger\hat{\Psi}_e\rangle$.

The lower part of Fig. 2 shows their dispersion relations for a typical excitation scheme $5s \to 5p \to 34s_{1/2}$ in ^{87}Rb. The coupling of the forward and backward propagating light field to the same intermediate level leads to a symmetric behavior of the bands and results in a linear dispersion. The solution at $k = 0$ presents a superposition of both bands, which results in a cancellation of the Rydberg part in the polaritons and a crossing of the bands at that point [26]. The surrounding bands like the one shown in the upper part of Fig. 2 are separated by a large band gap compared to the energy scales of the dark states so that we can focus our attention on the bands close to zero energy.

In the following, we transform the eigenstates of Eq. (2) into localized Wannier functions $\mathbf{w}_j(z) = (1/\sqrt{N})\sum_k e^{-ikaj}\boldsymbol{\phi}_k(z)$, resulting in bosonic creation operators $a_i^\dagger = \int dz\mathbf{w}(z)\mathbf{\Psi}(z)$ for the upper band and the analogous operators b_i for the lower band. Additionally, we consider pumping on the first lattice site with strength p, describing the driving with a coherent light field from the left. In the Wannier basis, the Hamiltonian has the form

$$\begin{aligned} H_0 = &-\sum_{i,j} J_{i,j}(\hat{a}_i^\dagger\hat{a}_j - \hat{b}_i^\dagger\hat{b}_j + \text{H.c.}) \\ &+ (2\epsilon - \beta)\sum_i \hat{b}_i^\dagger\hat{b}_i + \beta\sum_i \hat{a}_i^\dagger\hat{a}_i \\ &+ p(\hat{a}_1^\dagger + \hat{a}_1 + \hat{b}_1^\dagger + \hat{b}_1). \end{aligned} \tag{3}$$

The first line in Eq. (3) describes hopping between the sites with a strength of $J_{i,j}$, which can be written in terms of the hopping length m as J_m with $|i-j| = ma$. The strength of J_m can be tuned by the control and probe laser, i.e., the Rabi frequency Ω and the coupling strength $g(z)$. It is important to note that the scaling of $J_{i,j}$ with the distance $|i-j|$ does not follow an exponential decay but a power law asymptotically decaying like $|i-j|^{-2}$, which arises from the linear dispersion of the bands at around $k \approx 0$. Hence, we cannot approximate the system by a nearest-neighbor hopping J_1, which is possible when considering different level schemes [27].

The term β takes the role of a chemical potential and can be tuned by the frequency of the pump laser. We choose $\beta = 0.45\gamma$ so that $J_1/(2\epsilon - \beta) \ll 1$, which leads to a strong detuning of the lower band and allows us to neglect it in the following.

Let us now consider the consequences of the van der Waals interaction $V(z) = C_6/z^6$ between atoms in the Rydberg state on our system to see if the assumptions we

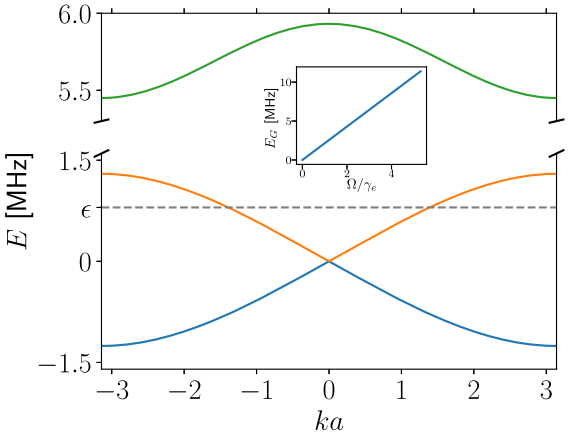

FIG. 2. Dispersion relation for polaritons close to zero energy for $\Omega/2\pi = 18$ MHz, $\delta_e/2\pi = 20$ MHz, $\gamma_e/2\pi = 6$ MHz, and $a = 532$ nm. We obtain two dark-state polariton bands and exemplarily show a bright state polariton band. The dashed gray line indicates the average energy ϵ of the upper dark-state polariton. The inset shows the scaling of the band gap with Ω.

made so far still hold true. The repulsive nature of the interaction leads to a blockade radius inside the lattice which is defined through the strength of the hopping J_1 between different sites and the van der Waals coefficient C_6 for the chosen Rydberg state $\tilde{r}_b = \sqrt[6]{(C_6/J_1)}$, similar to the conventional Rydberg blockade for stationary atoms [28]. An important consequence of the van der Waals force is the two-photon detuning for atoms in the vicinity of an already excited atom which exceeds the EIT linewidth of the system at a characteristic distance $r_b = \sqrt[6]{(C_6|\Delta|/\Omega^2)}$. Below that distance the EIT window brakes and photons can get absorbed into the intermediate state of the atoms. This causes a scattering of the photons and restricts the creation of a new polariton only to sites outside r_b and it also allows us to restrict the pumping term in Eq. (3) to the first site of the lattice [29]. For the chosen parameters, we find $\tilde{r}_b \approx 5a$ and $r_b \approx 2a$; i.e., the Rydberg blockade screens the breakdown of the EIT resonance. In this regime, the only consequence of r_b is a regularization of the van der Waals interaction potential, which results in a two-body interaction V_{ij} according to

$$V_{ij} = \frac{C_6}{2} \int dz dz' \frac{\mathbf{w}_i^*(z)\mathbf{w}_j^*(z')\mathbf{w}_j(z')\mathbf{w}_i(z)}{r_b^6 + |z - z'|^6}. \tag{4}$$

Furthermore, $r_b > a$ prevents the formation of more than one dark-state polariton per site. We implement this restriction by choosing Pauli operators $\sigma^{-(+)}$ for the annihilation (creation) operators $a^{(\dagger)}$ in Eq. (3). In this picture, the spin 1/2 states $|\uparrow\rangle_i$ and $|\downarrow\rangle_i$ correspond to the existence or absence of a dark-state polariton at site i, respectively. At distances larger than $\tilde{r}_b$, the interaction energy is small compared to the band gap between the dark-state polaritons and the other bands so that the single-band approximation still holds true. Putting everything together gives us an extended Bose-Hubbard Hamiltonian for interacting dark-state polaritons:

$$H = -\sum_{i,j} J_{i,j}\sigma_i^+\sigma_j^- + p(\sigma_1^+ + \sigma_1^-) + \beta\sum_i \sigma_i^+\sigma_i^- + \sum_{i,j} V_{ij}\sigma_i^+\sigma_j^+\sigma_i^-\sigma_j^-. \tag{5}$$

So far we have neglected the second natural dissipation channel in our system in the form of the spontaneous decay from the Rydberg state. To describe the dynamics of the open quantum system under the condition of Markovianity, we can use the Lindblad form of the differential equation $(d/dt)\rho = \mathcal{L}\rho$ with the Liouvillian $\mathcal{L}$ being the generator of the dynamics [30], i.e.,

$$\mathcal{L}(\rho) = -i[H(t), \rho(t)] + \sum_j \left(c_j \rho c_j^\dagger - \frac{1}{2}\{c_j^\dagger c_j, \rho\} \right). \tag{6}$$

The spontaneous emission from the Rydberg state also affects the polaritons and is described by the jump operators $c_i = \sqrt{\gamma}\sigma_-^{(i)}$ for each site i and an effective decay rate of $\gamma = \int dz |w_r^{(i)}(z)|^2 \gamma_r = 12.5$ kHz, with γ_r being the decay rate of the Rydberg state [31]. Here we have neglected the decay from the intermediate state, as this process is orders of magnitude slower for dark-state polaritons. Additionally, to account for photons leaving the system along the propagation axis, we add another dissipation channel with jump operators $c_{1(,N)} = \sqrt{\gamma_{\text{out}}}\sigma_-^{1(,N)}$ that only applies on the first and last site of the lattice. Here, we consider the case where $\gamma_{\text{out}} = J_1$; i.e., the coupling to the outside has the same strength as the internal nearest-neighbor hopping. This also allows us to compute the output photon intensity in terms of the internal dynamics of the polaritons in the system, providing a similar approach as the input-output formalism in, for example, cavity QED systems [32,33]. We define the (normalized) output intensity as $I_{\text{out}} = J_1\langle\sigma_N^+\sigma_N^-\rangle$. Similar processes can also be defined for the other sites but show an insignificant influence on the overall dynamics.

We perform exact numerical simulations of the system for site numbers up to $N = 10$ via the wave-function Monte Carlo method using the QuTiP library [34], which amounts to an average of about two polaritons inside the system. In all our simulations, we choose the initial state to have no polaritons in the system. However, this approach is limited to studying system sizes of at most $N = 20$ due to the exponential growth of the Hilbert space [35]. To analyze the output for larger lattices, we use a variational approach [36,37] starting with a product ansatz for the density matrix,

$$\rho = \prod_{i=1}^N \rho_i = \frac{1}{2}\prod_{i=1}^N \left(1 + \sum_{\mu\in\{x,y,z\}} \alpha_\mu \sigma_\mu^i\right), \tag{7}$$

with ρ_i as the density matrix for each lattice site and α_μ as our variational parameters. This product state is then restricted to a blockade constraint for the polaritons, such that there is only one polariton inside a blockade radius r_b, i.e., $\sum_{i-r_b<j<i+r_b}\langle\sigma_+^{(j)}\sigma_-^{(j)}\rangle \leq 1$ for all sites i. This approach is equivalent to the hard sphere correlation function used in the analysis of coherently driven Rydberg gases [38].

For the variational integration of the quantum master equation, we use an implicit midpoint method [37]. To reduce the number of variational parameters in a single optimization, we evolve the system from t to $t + \Delta t$ by minimizing the parameters for one site and hold every other site constant [39]. This procedure is repeated for all sites before moving on to the next time step. For the variational optimization we use the norm D_i for each site i given by

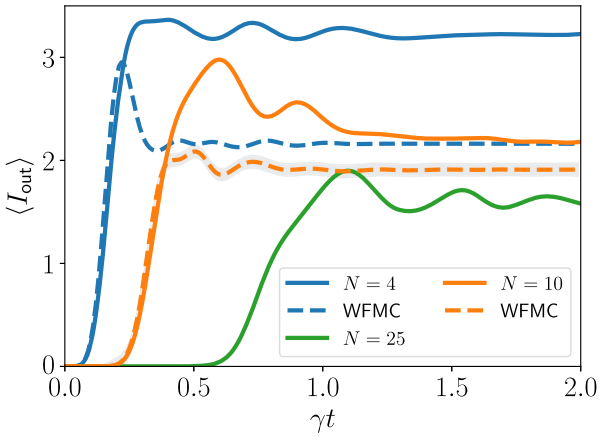

FIG. 3. Intensity output $\langle I_{\text{out}} \rangle$ for different system sizes for a pump strength of $p = 10\gamma$. For smaller system size ($N = 4$, 10) the variational approach (solid lines) is compared to wave-function Monte Carlo (WFMC) simulations (dashed lines). The shaded region shows the statistical error of the WFMC simulations for 500 trajectories.

$$D_i = \sum_{j \neq i} \Big\| -\frac{\tau}{2}\mathcal{L}[\rho_i(t+\tau)\rho_j(t) + \rho_{ij}(t)] + \rho_i(t+\tau)\rho_j(t) - \rho_{ij}(t) \Big\|_1 \to \min, \tag{8}$$

where $\| \cdot \|_1$ denotes the trace norm given by $\mathrm{Tr}\{|\cdot|\}$. Additionally, we add constraints to the minimization to enforce the positivity of the density matrix $\rho_i \geq 0$ and to enforce the blockade of the polaritons.

Figure 3 shows the intensity output I_{out} for different lattices sizes N. Additionally, we benchmark the variational results against wave-function Monte Carlo simulations. We find that the two are in good agreement for $N = 10$, with the remaining difference being caused by short-range correlation between the ends. This effect is much stronger for $N = 4$ and diminishes for larger system sizes. Having demonstrated the viability of the variational approach, we now turn to the variational simulation of larger system sizes. Figure 4 displays the dynamics of the polariton population on each site for a lattice size of $N = 40$. We observe that a significant portion of the polariton density remains confined to the initial pump site, with the rest of the population spreading throughout the system similar to a light cone, which is a consequence of the linear dispersion relation. Furthermore, we find that the Rydberg blockade has a significant effect on the output signal. Above $p \approx 10\gamma$ we do not see any further increase in the output as the polariton population leads a saturation of the hard sphere constraint.

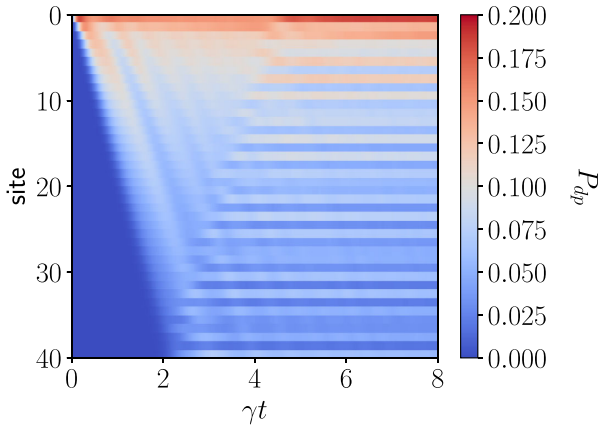

FIG. 4. Time evolution of the polariton population $P_{dp}^{(i)} = \langle \sigma_+^{(i)} \sigma_-^{(i)} \rangle$ of each site i in a lattice of size $N = 40$ for a pumping strength of $p = 10\gamma$.

Finally, we also want to look at the temporal correlations in the output intensity. For this, we let the system evolve until it reaches a steady state at time t_{ss}. At this time, we consider the effect of a quantum jump corresponding to a photon leaving the system, after which we let the system evolve for an additional time τ. Then, the probability to observe a second photon is described by the two-time correlation function,

$$g^{(2)}(\tau) = \frac{\langle \sigma_N^+(t_{\text{ss}})\sigma_N^+(t_{\text{ss}}+\tau)\sigma_N^-(t_{\text{ss}}+\tau)\sigma_N^-(t_{\text{ss}})\rangle}{\langle \sigma_N^+\sigma_N^-\rangle_{t_{\text{ss}}}^2} = \frac{1}{\langle \sigma_N^+\sigma_N^-\rangle_{\text{ss}}^2}\mathrm{Tr}\{\sigma_N^- e^{\mathcal{L}\tau}[\sigma_N^-\rho(t_{\text{ss}})\sigma_N^+]\sigma_N^+\}, \tag{9}$$

where we have used the cyclicity of the trace and the operators $\sigma_N^{+(-)}$ are only acting on the last site N of the lattice [40]. The van der Waals interaction ensures that all sites inside the blockade radius of the last site are in an unexcited state at the time of the first measurement. We use a self-consistent approach to identify this distance by adding the excitation probabilities of the other sites beginning from site $N-1$ until $\sum_{i=N-1}\langle \sigma_i^+\sigma_i^-\rangle = 1$ and set them back to the ground state. The blockaded region which is defined in that way is for smaller system size identical to our previous definition of the blockade radius. For larger system sizes, the radius is extended because it takes the consequences of the decay from the Rydberg state into account.

Figure 5 shows an extended antibunched region [$g^{(2)}(\tau) \approx 0$]. Its duration depends on the self-consistent blockade radius as well as the hopping strengths J_m. We also observe bunching that increases with the system size before the system recovers to its steady state $g^{(2)}(\tau) = 1$. These findings underline the possibility of using Rydberg polariton systems to generate strongly correlated photon streams, similar to what has been discussed for free-space systems [29].

In summary, we have demonstrated the possibility to treat large many-body systems of driven-dissipative systems of strongly interacting Rydberg polaritons using a variational approach. Deriving an extended Bose-Hubbard

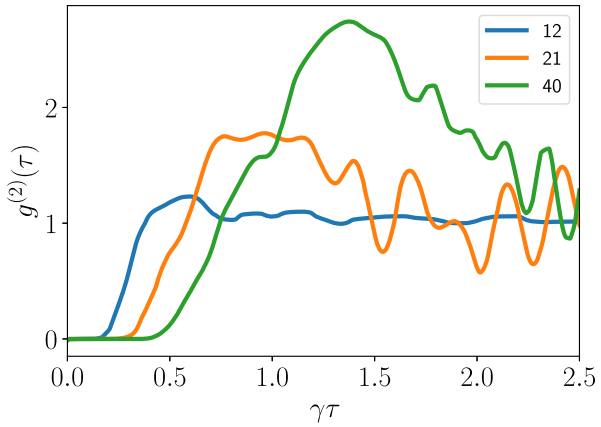

FIG. 5. Two-time correlation function $g^{(2)}(\tau)$ of the output signal from the last site of the lattice for different system sizes N.

model with long-range hopping and interactions, we observe that the propagation of photons through a lattice can yield strong correlations between the particles. The variational approach proved to be a good approximation for the dynamics especially for larger system sizes. Our work presents a first look into the driven-dissipative transport of Rydberg polaritons and paves the way for future investigations of different driving scenarios and extensions to free-space polaritons in the form of a suitable continuum limit.

We thank H. P. Büchler for fruitful discussions. This work was funded by the Volkswagen Foundation, by the Deutsche Forschungsgemeinschaft (DFG, German Research Foundation) within SFB 1227 (DQ-mat, Project No. A04), SPP 1929 (GiRyd), and under Germany's Excellence Strategy—EXC-2123 QuantumFrontiers—390837967.

*tim.pistorius@itp.uni-hannover.de

[1] M. Müller, S. Diehl, G. Pupillo, and P. Zoller, in *Advances in Atomic, Molecular, and Optical Physics*, Vol. 61, edited by P. Berman, E. Arimondo, and C. Lin (Academic Press, New York, 2012), pp. 1–80.
[2] L. M. Sieberer, M. Buchhold, and S. Diehl, Rep. Prog. Phys. **79**, 096001 (2016).
[3] H. Weimer, A. Kshetrimayum, and R. Orús, arXiv:1907.07079.
[4] I. Friedler, D. Petrosyan, M. Fleischhauer, and G. Kurizki, Phys. Rev. A **72**, 043803 (2005).
[5] Y. O. Dudin and A. Kuzmich, Science **336**, 887 (2012).
[6] T. Peyronel, O. Firstenberg, Q.-Y. Liang, S. Hofferberth, A. V. Gorshkov, T. Pohl, M. D. Lukin, and V. Vuletić, Nature (London) **488**, 57 (2012).
[7] O. Firstenberg, T. Peyronel, Q.-Y. Liang, A. V. Gorshkov, M. D. Lukin, and V. Vuleti, Nature (London) **502**, 71 (2013).
[8] S. H. Cantu, A. V. Venkatramani, W. Xu, L. Zhou, B. Jelenkovi, M. D. Lukin, and V. Vuleti, arXiv:1911.02586.
[9] S. Baur, D. Tiarks, G. Rempe, and S. Dürr, Phys. Rev. Lett. **112**, 073901 (2014).
[10] H. Gorniaczyk, C. Tresp, J. Schmidt, H. Fedder, and S. Hofferberth, Phys. Rev. Lett. **113**, 053601 (2014).
[11] D. Tiarks, S. Baur, K. Schneider, S. Dürr, and G. Rempe, Phys. Rev. Lett. **113**, 053602 (2014).
[12] D. Tiarks, S. Schmidt-Eberle, T. Stolz, G. Rempe, and S. Drr, Nat. Phys. **15**, 124 (2019).
[13] A. V. Gorshkov, S. R. Manmana, G. Chen, J. Ye, E. Demler, M. D. Lukin, and A. M. Rey, Phys. Rev. Lett. **107**, 115301 (2011).
[14] J. Otterbach, M. Moos, D. Muth, and M. Fleischhauer, Phys. Rev. Lett. **111**, 113001 (2013).
[15] P. Bienias, S. Choi, O. Firstenberg, M. F. Maghrebi, M. Gullans, M. D. Lukin, A. V. Gorshkov, and H. P. Büchler, Phys. Rev. A **90**, 053804 (2014).
[16] M. J. Gullans, J. D. Thompson, Y. Wang, Q.-Y. Liang, V. Vuletić, M. D. Lukin, and A. V. Gorshkov, Phys. Rev. Lett. **117**, 113601 (2016).
[17] M. Fleischhauer and M. D. Lukin, Phys. Rev. Lett. **84**, 5094 (2000).
[18] M. Fleischhauer, A. Imamoglu, and J. P. Marangos, Rev. Mod. Phys. **77**, 633 (2005).
[19] J. D. Pritchard, D. Maxwell, A. Gauguet, K. J. Weatherill, M. P. A. Jones, and C. S. Adams, Phys. Rev. Lett. **105**, 193603 (2010).
[20] H. Schempp, G. Günter, C. S. Hofmann, C. Giese, S. D. Saliba, B. D. DePaola, T. Amthor, M. Weidemüller, S. Sevinçli, and T. Pohl, Phys. Rev. Lett. **104**, 173602 (2010).
[21] N. Jia, N. Schine, A. Georgakopoulos, A. Ryou, L. W. Clark, A. Sommer, and J. Simon, Nat. Phys. **14**, 550 (2018).
[22] P. Bienias and H. P. Büchler, J. Phys. B **53**, 054003 (2020).
[23] I. Bloch, J. Dalibard, and W. Zwerger, Rev. Mod. Phys. **80**, 885 (2008).
[24] F. E. Zimmer, J. Otterbach, R. G. Unanyan, B. W. Shore, and M. Fleischhauer, Phys. Rev. A **77**, 063823 (2008).
[25] M. Fleischhauer and M. D. Lukin, Phys. Rev. A **65**, 022314 (2002).
[26] I. Iakoupov, J. R. Ott, D. E. Chang, and A. S. Sørensen, Phys. Rev. A **94**, 053824 (2016).
[27] M. Mašalas and M. Fleischhauer, Phys. Rev. A **69**, 061801 (R) (2004).
[28] D. Jaksch, J. I. Cirac, P. Zoller, S. L. Rolston, R. Côté, and M. D. Lukin, Phys. Rev. Lett. **85**, 2208 (2000).
[29] E. Zeuthen, M. J. Gullans, M. F. Maghrebi, and A. V. Gorshkov, Phys. Rev. Lett. **119**, 043602 (2017).
[30] H.-P. Breuer and F. Petruccione, *The Theory of Open Quantum Systems* (Oxford University Press, Oxford, 2002).
[31] D. B. Branden, T. Juhasz, T. Mahlokozera, C. Vesa, R. O. Wilson, M. Zheng, A. Kortyna, and D. A. Tate, J. Phys. B **43**, 015002 (2010).
[32] T. Caneva, M. T. Manzoni, T. Shi, J. S. Douglas, J. I. Cirac, and D. E. Chang, New J. Phys. **17**, 113001 (2015).
[33] C. W. Gardiner and M. J. Collett, Phys. Rev. A **31**, 3761 (1985).

[34] J. Johansson, P. Nation, and F. Nori, Comput. Phys. Commun. **184**, 1234 (2013).
[35] M. Raghunandan, J. Wrachtrup, and H. Weimer, Phys. Rev. Lett. **120**, 150501 (2018).
[36] H. Weimer, Phys. Rev. Lett. **114**, 040402 (2015).
[37] V. R. Overbeck and H. Weimer, Phys. Rev. A **93**, 012106 (2016).
[38] H. Weimer, R. Löw, T. Pfau, and H. P. Büchler, Phys. Rev. Lett. **101**, 250601 (2008).
[39] V. R. Overbeck, M. F. Maghrebi, A. V. Gorshkov, and H. Weimer, Phys. Rev. A **95**, 042133 (2017).
[40] C. Gardiner and P. Zoller, *Quantum Noise* (Springer-Verlag, Berlin, 2004).